

# Para-amino Benzoate Ferroxane/Chitosan Nanocomposite as a Promising Adsorbent for Lead Wastewater Treatment

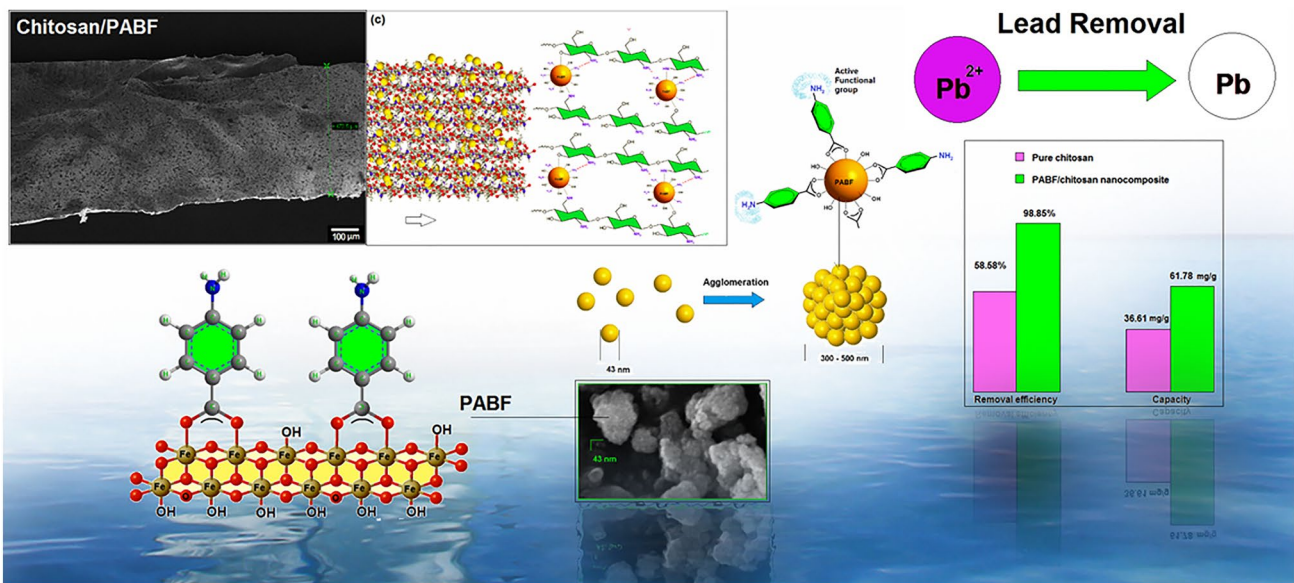
Rozita M. Moattari<sup>1,2</sup> · Safoora Rahimi<sup>1</sup> · Laleh Rajabi<sup>1</sup> · Ali Ashraf Derakhshan<sup>3</sup>

Received: 24 June 2022 / Revised: 19 September 2022 / Accepted: 24 September 2022 / Published online: 11 October 2022  
© University of Tehran 2022

## Abstract

This research study focuses on adsorption of lead ions from aqueous solution by PABF (para-amino benzoate ferroxane)/chitosan nanocomposites. Response surface methodology (RSM) based on the three-variable-three-level Box–Behnken design, was employed to optimize the influences of major operating variables. Three independent variables, namely, initial solution pH (3–6), adsorbent mass (0.002–0.09 g), and initial Pb(II) concentration (50–150 mg/L) were consecutively coded as  $X_1$ ,  $X_2$  and  $X_3$  at three levels (–1, 0 and 1). Regression analysis indicated good fit of the experimental data to the second-order polynomial model with a coefficient of determination ( $R^2$ ) value of 0.986 and  $F$  value of 70.24. The highest lead removal efficiency of 98.27% was found at optimum conditions of 5.99, 0.04 g and 74.48 mg/L, respectively, for initial solution pH, adsorbent dosage and initial concentration of Pb(II) ions. Such a removal efficiency was in good coincidence with the model prediction (99.93%). The PABF/chitosan nanocomposites were characterized by FTIR, DLS, and SEM analyses and final Pb(II) concentrations were analysed using Inductively Coupled Plasma Atomic Emission Spectrometer. In addition, the equilibrium data fitted well to the Langmuir isotherm.

## Graphical Abstract



✉ Rozita M. Moattari  
rozitammoattary@gmail.com

Extended author information available on the last page of the article

## Highlights

- PABF/chitosan nanocomposites were synthesized and characterized
- Carboxylate ferroxanes nanocomposites were used as sorbents for lead removal
- Box–Behnken method was used to design the experiments and optimization the process
- The equilibrium data fitted well to the Langmuir isotherm
- The monolayer adsorption process was dominated

**Keywords** Nanocomposite · Adsorption · Response surface methodology · Chitosan · Carboxylate–ferroxane · Box–Behnken design

## Introduction

Environmental pollution from the release of toxic heavy metals due to the proliferation of industrial activities is reaching dangerous levels (Amini et al. 2008). These dangerous levels have occurred especially in lakes, marine, rivers, underground water, and (un)treated industrial waste waters (Amini et al. 2008; Soylak et al. 2008). Harmful effects of heavy metals on the environment and public health are due to their toxic nature, non-biodegradability, and carcinogenic effect. Thus, it is vital to deplete heavy metals from the aquatic environment (Abou-Shady et al. 2012; Mert et al. 2013; Celebi et al. 2020). Among the heavy metals, Pb(II) is one of the most important metals in terms of health risks based on environmental regulations (Dolgen et al. 2007; Tan et al. 2012; Zheng et al. 2016; Yap et al. 2017). Various technologies such as adsorption, chemical precipitation, electrochemical technique, etc., have been used for lead removal (Tan et al. 2012; Gholami et al. 2014; Muñoz et al. 2016). The adsorption is one of the most interesting and effective techniques because of its accessibility of different adsorbents, low cost, and easy operational condition (Mert et al. 2013; Şener et al. 2014; Tekin et al. 2011; Hui and Ye 2016). A wide variety of adsorbents such as basic oxygen furnace slag (Kim et al. 2020), magnetic  $\text{Fe}_3\text{O}_4/\text{MnO}_2$  core–shell (Yang et al. 2020), mesoporous coral limestones (Nkutha et al. 2020),  $\alpha\text{-FeOOH}/\text{Cellulose}/\text{TiO}_2$  (Mahmoud and Abdelwahab 2020), octylamine functionalized vermiculite (Ahmed et al. 2020), melamine-grafted chitosan (Ge and Du 2020), chitosan–boehmite composite (Chen et al. 2020), magnetic sporopollenin supported polyaniline, (Mosleh et al. 2022), waste biomass based bioadsorbent (BahadurPal et al. 2022), calcium carbonate (Fiorito et al. 2022), pistachio, peanut, and almond shells (Kayranli et al. 2022), brewed tea waste (Celebi et al. 2020), natural Walnut Shell (Celebi and Gok 2017), etc. for the removal of lead from the aqueous medium have been studied. Among the various adsorbents, biopolymers such as chitosan are known as noteworthy adsorbents (Wan Ngah et al. 2011). Chitosan is a good adsorbent due to its low cost, biocompatibility, biodegradability, poor

solubility in aqueous solutions and high content of  $\text{NH}_2$  and OH functional groups as active adsorption sites (Gerente et al. 2007; Valderruten et al. 2014; Ogunlaja et al. 2014; Kołodziejka et al. 2017). Chemical modifications through the formation of chitosan composites lead to increase in chemical and mechanical features of reinforced chitosan films. Hence, this modification method has received considerable attention, greatly studied, and widely published in the literature (Zheng et al. 2016; Chiou et al. 2004). Previous reports indicated that chitosan adsorption performance could be improved using cross-linkers such as formaldehyde, glyoxal, glutaraldehyde, isocyanates, etc. (Crini and Badot 2008). In addition, various chitosan-based composites have been prepared using bentonite (Ngah et al. 2010), montmorillonite (Wang and Wang 2007), polyurethane (Lee et al. 2009), perlite (Kalyani et al. 2005), activated clay (Chang and Juang 2004), kaolinite, polyvinyl chloride, polyvinyl alcohol (Zhu et al. 2010), and oil palm ash (Hasan et al. 2008). The results disclosed that the chitosan-based composites exhibit a higher adsorption capacity and improved acid resistance (Boddu et al. 2008). Tran et al. stated the magnetite nanoparticles–chitosan composites are promising adsorbents for the uptake of Ni(II) and pb(II) (Tran et al. 2010).

It is clearly indicated that use of nanoparticles in the polymeric structure of nanocomposites eliminates the major drawback of nanoparticle in water treatment applications; from this point of view secondary pollution due to nanoparticle dispersion can be completely controlled (Liu et al. 2008).

As mentioned above, many adsorbents have been investigated to remove lead from water/wastewater. However, the introduction of new adsorbents continues in this field and researchers are looking for adsorbents to solve the drawbacks and defects of previous adsorbents. It is desirable for an adsorbent that, in addition to good adsorption performance, cannot cause secondary pollution in water, its separation is easy from water after the adsorption process, can show good adsorption performance in the neutral pH range, and its synthesis is facile (especially on a large scale), to be

prepared from available materials, etc. According to these points, many previously introduced adsorbents such as nanoparticles are difficult to separate from water due to their easy dispersibility in water. They are synthesized from expensive materials that make their use on a large scale challenging. They do not have chemical stability in the range of pH 2–4. However, in this study, an adsorbent has been introduced to solve the problems mentioned above as much as possible. In the present study, attention is paid to a new nanocomposite for lead adsorption from aqueous solutions. To this end, para aminobenzoate ferroxane (PABF) nanoparticles thanks to the existence of the  $\text{NH}_2$  functional group on the surface of nanoparticles have been selected, prepared and utilized as a reinforcing agent to promote the adsorption characteristics of chitosan film. Coexisting of various functional groups in a united adsorption structure made the nanocomposites into a high potential adsorbent. The effects of various parameters viz. initial solution pH, nanoparticle mass, and initial concentration of  $\text{Pb}^{2+}$  ions were probed by Box–Behnken design methodology. In addition, the optimum parameters were found to attain the highest adsorption efficiency. Experimental data were analyzed by adsorption isotherms including Freundlich and Langmuir models.

## Experimental Procedure

### Chemicals and Materials

Low molecular weight chitosan powder was procured from Sigma-Aldrich (USA). Analytical-grade caustic soda (NaOH), nitric acid ( $\text{HNO}_3$ ), iron (II) chloride tetrahydrate, hexamethylenetetramine, sodium nitrate, acetic acid ( $\text{CH}_3\text{COOH}$ ), ethanol, 4-Aminobenzoic acid, and lead stock solution (NIST  $\text{Pb}(\text{NO}_3)_2$  in  $\text{HNO}_3$  1000 mg/L) were provided from Merck (Germany). All the required solutions were prepared by dissolving the chemical reagents in deionized (DI) water.

### Fabrication of PABF/Chitosan Nanocomposites

Lepidocrocite, the precursor of PABF, was first prepared through the reaction of  $\text{FeCl}_2 \cdot 4\text{H}_2\text{O}$ ,  $\text{NaNO}_3$ , and hexamethylenetetramine (Moattari et al. 2014). The ferroxane nanoparticles used in this research were prepared according to a previously published method (Moattari et al. 2014). Briefly, 4.82 g (0.042 mol) lepidocrocite and 6 g 4-Aminobenzoic acid were mixed with 500 ml deionized water in a 1000 ml flat-bottomed flask. The formed suspension was exposed to ultrasound waves for 20 min in a bath-type sonicator. The

suspension was then refluxed for 20 h at its boiling temperature after which it was cooled at ambient temperature and centrifuged for 30 min at 4000 rpm. To remove unreacted 4-Aminobenzoic acids, the separated precipitate was washed several times with 200 ml of ethanol. The wet precipitate was centrifuged, dried in an oven at  $80^\circ\text{C}$ , ground and sieved through the mesh No. 60. Afterwards, the modified PABF/chitosan adsorbent nanocomposites were synthesized by the solution-casting method. The PABF/chitosan solutions were provided as described below: 0.2 g of chitosan powder and a certain quantity of PABF were dissolved in 1% (v/v) acetic acid solution. The ultrasound waves were propagated to the obtained suspension for 10 min to ensure complete dissolution of the solutes. Table S1 presents the synthesis details of nanocomposites.

The prepared solution was incubated at 180 rpm and room temperature for 24 h and then pre-heated in an oven at  $50^\circ\text{C}$  for 48 h to release the trapped air bubbles. Afterwards, proper films were prepared by knife-casting the resulting solution on some glass plates and allowed to dry at room temperature. To neutralize the excess acid and also minimize the water-solubility of the films, the films were submerged in 1 M NaOH alkaline solution for 1 h. Later, they were exhaustively rinsed with DI water and then left to dry at ambient temperature for 24 h.

### Characterizations

Fourier transform infrared (FTIR), dynamic light scattering (DLS), and scanning electron microscopy (SEM) techniques were applied to characterize the PABF/chitosan nanocomposites. FTIR spectra were taken at wavenumbers of  $400\text{--}4000\text{ cm}^{-1}$  using KBr technique at ambient temperature (Bruker alpha, German). A DLS analyzer (Malvern Instruments, UK) was employed to obtain particle size distribution of nanoparticles. To perform a DLS analysis, 5% W/V (nanoparticle/water) samples were prepared. Microstructures of all

**Table 1** Synthesis details of PABF/chitosan nanocomposite Variables and their levels for Pb(II) adsorption by PABF/chitosan nanocomposites

Variable	Level		
	Lower	Central	Upper
pH	3	4.5	6
$C_n$ (g)	0.002	0.046	0.09
$C_0$ (mg/L)	50	100	150

samples were observed using Philips XL-30S FEG and LEQ 1450 VP, scanning electron microscopy.

## Adsorption Tests

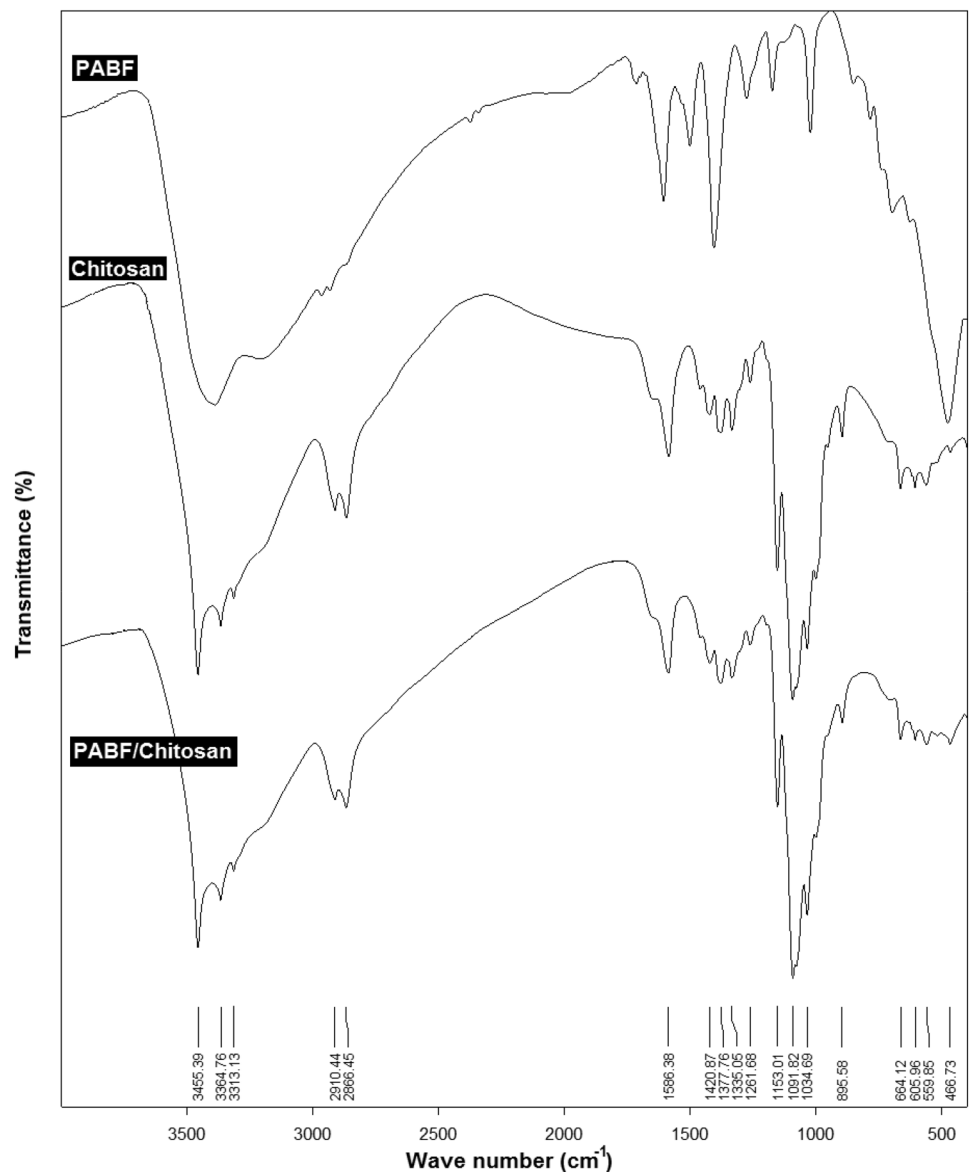
The required lead solutions with appropriate concentrations were provided by adding DI water to the standard lead solution (1000 mg/L). 0.002 g adsorbent was poured into 25 ml of the specified concentration of Pb(II) solutions in a 100 ml Erlenmeyer flask. The adsorbent-solution mix was then agitated at 180 rpm for 24 h at ambient temperature to reach adsorption equilibrium conditions. Based on preliminary removal experiments, the effect of contact times of 30 min to 30 h were evaluated on the removal efficiency. The results showed a contact duration of 24 h was enough to reach equilibrium. Therefore,

all adsorption tests were performed under a constant contact time of 24 h. The pH of the solutions were adjusted using 1 M HNO<sub>3</sub> and 1 M NaOH. The nanocomposite adsorbent was then separated from aqueous solutions by a vacuum filtration system. The supernatants were analyzed utilizing an inductively coupled plasma atomic emission spectrometer (ICP-OES simultaneous–Varian VISTA-PRO Model). The Lead removal efficiency was determined according to Eq. (1) and adsorbent capacity was calculated according to Eq. (2):

$$R\% = \left( \frac{C_0 - C_t}{C_0} \right) \times 100 \quad (1)$$

$$q_t = \frac{(C_0 - C_t) \times V}{m} \quad (2)$$

**Fig. 1** FTIR spectra of PABF nanoparticle, pure chitosan and PABF/chitosan nanocomposite



where  $R\%$  is removal efficiency,  $q_t$  is the quantity of adsorbed lead (mg/g) at a specified time  $t$ .  $C_0$  and  $C_t$  stand for the initial and final Pb(II) ion concentrations (mg/L) in the solution, respectively.  $m$  and  $V$  stand for the dosage of the adsorbent (g) and volume of solution (L), respectively.

### Box–Behnken Design of Experiment

Response surface methodology (RSM) is a beneficial multivariate technique that can achieve to an optimized process through a response function and it proposed to solve the disadvantages of one-factor-at-a-time approach (Tavares et al. 2009; Bandaru et al. 2006; Dil et al. 2017). In this work, Pb(II) uptake by PABF/chitosan nanocomposite was examined by applying three-variable-three-level Box–Behnken design (BBD) from the RSM. The BBD is known as a quadratic design approach in which each independent variable is placed at one of three equally spaced values (Ay et al. 2009; Rahimi et al. 2015). Table 1 presents experimental variables including initial pH, nanoparticle amount ( $C_n$ ), initial concentration of  $Pb^{2+}$  ions ( $C_0$ ) and their levels. Various parameters such as initial concentration, solution pH, adsorbent dose, contact time, stirring speed, temperature, etc. affect the adsorption amount. To select the most influential parameters, a screening pretest was performed with the Plackett–Burman method. The results showed that the initial concentration, solution pH, and adsorbent dose were the three most effective parameters, and therefore they were chosen for further study and optimization of the adsorption process by the BBD method. The software Design Expert 8 trial version was utilized for the experimental design, the data analysis, determination of the coefficients, and the graph plotting.

Three three-level independent variables denoted as  $X_1$ ,  $X_2$  and  $X_3$  were considered for statistical calculations.

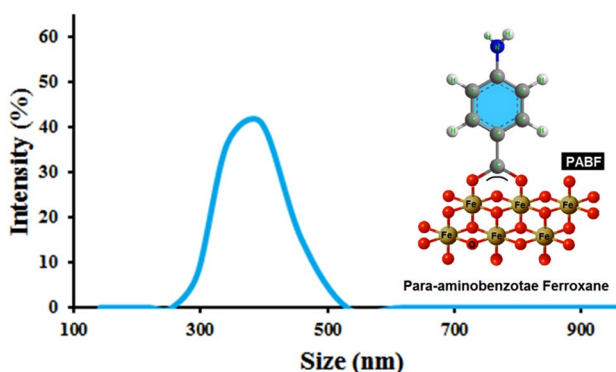


**Fig. 2** Particles size distributions of the PABF nanoparticles by dynamic light scattering and molecular structure of the PABF nanoparticles

Three levels were coded at values of  $-1$ ,  $0$  and  $+1$ . The effects of  $X_1$ ,  $X_2$  and  $X_3$  on the lead removal efficiency were investigated.

The reason for choosing the concentration range was because the effluent of some industries is in the range of 50–150 ppm. Therefore, to check the applicability of the adsorbent introduced in this study, the same concentration range was selected. The reason for choosing the pH range was that first, lead precipitates at pHs above 7 and it is impossible to check the removal through adsorption. Secondly, many industrial effluents containing lead do not have a pH lower than 2. As a result, pH 3 to 6 was selected for the study. The reason for choosing the introduced range for the adsorbent dose was that, firstly, nanoabsorbents do not need high doses due to their high specific surface area. Secondly, choosing higher doses creates an economic challenge in the adsorption process. Third, in the preliminary tests, doses outside the introduced range were also tested, which either had a weak response or did not show much difference from the selected range.

## Results and Discussion

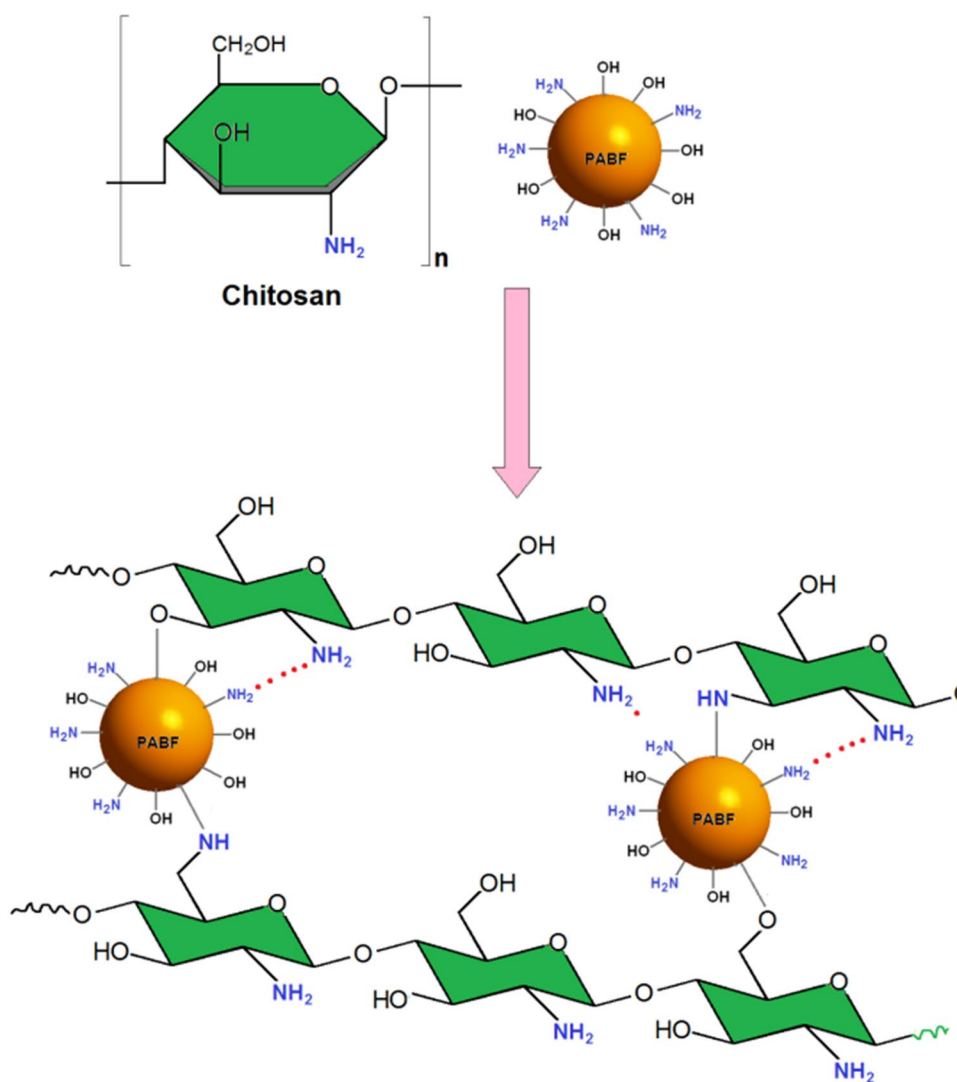
### Characterization of Adsorbents

#### Identification of Chemical Bonds by FTIR Analysis

Figure 1 depicts the FTIR spectra of pure chitosan, PABF nanoparticle, and PABF/chitosan nanocomposite. The absorption bands at  $3455\text{ cm}^{-1}$  are assigned to the vibration of  $H_2O$  molecules. As seen in the PABF spectrum, the two index absorption bands at  $1404$  and  $1500\text{ cm}^{-1}$  are related to the symmetric and asymmetric stretching vibrations of carboxylates. The emergence of such bands indicates the carboxylate bonding between the carboxylic acid groups with the surface of the lepidocrocite nanoparticles. The band at  $1605\text{ cm}^{-1}$  also corresponds to the stretching vibrations of the aromatic  $C=C$  bonds that broadening this absorption band at  $1640\text{ cm}^{-1}$  belongs to the bending vibrations of the amine  $N-H$  groups. The band at  $3370\text{ cm}^{-1}$  is related to the stretching vibrations of  $NH$  groups. (Moattari et al. 2014).

No evident differences are observed between the two spectra of chitosan and PABF/chitosan nanocomposite. As a matter of fact, at the low concentrations of PABF in nanocomposite (PABF/chitosan), the intensity of index bands for PABF decreased and covered by index bands of chitosan. Only the intensity and position of some absorption bands have changed a little and at the wavenumber of  $475\text{ cm}^{-1}$  (the strongest band of PABF), a difference can be

**Fig. 3** The PABF/chitosan nanocomposite structure made from chitosan biopolymer and PABF nanoparticles



seen between chitosan and PABF/chitosan nanocomposite spectra.

### DLS Analysis of PABF Nanoparticles

Particle size distribution of PABF nanoparticle determined by DLS is depicted in Fig. 2. The average particle size of PABF was obtained 260–520 nm. The PABF particles provide numerous surface active bonding sites that can cause to the tendency of agglomeration and therefore, the DLS technique cannot determine the size of the single particles.

### SEM Analysis

Figure 3 illustrates the PABF/chitosan nanocomposite structure fabricated from chitosan and PABF nanoparticles, schematically. PABF nanoparticles with  $\text{NH}_2$  and OH groups on their surface, link the chains of chitosan biopolymer through the chemical interaction (covalent bonds) and physical

interaction (hydrogen bonds). In fact, these nanoparticles play the role of adsorbent as well as the reinforcing agent in chitosan matrix.

An SEM image of the PABF nanoparticles is shown in Fig. 4. As can be seen, agglomerates of different sizes of 300–500 nm are formed. The main morphology is in the form of particles with rounded corners. The PABF nanoparticles have agglomerated due to the existence of strong interactions (hydrogen bonding) between the functional groups. The average particle size of PABF nanoparticles is about 43 nm and their surface is covered by  $\text{NH}_2$  groups.

Figure 5 presents the SEM images of surface and a cross section of PABF/chitosan nanocomposite. An approximate thickness of 470  $\mu\text{m}$  was obtained for the chitosan film. The SEM micrograph indicates the uniform distribution of PABF nanoparticles and agglomerates through the surface of the chitosan polymeric film.

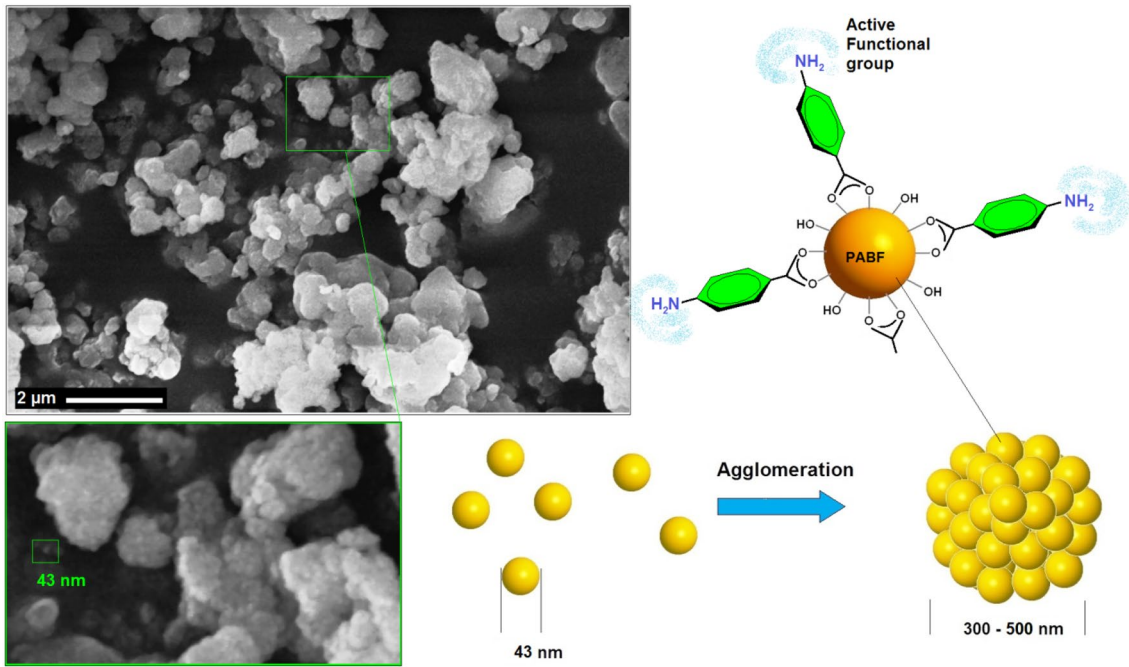


Fig. 4 SEM image of the PABF nanoparticles

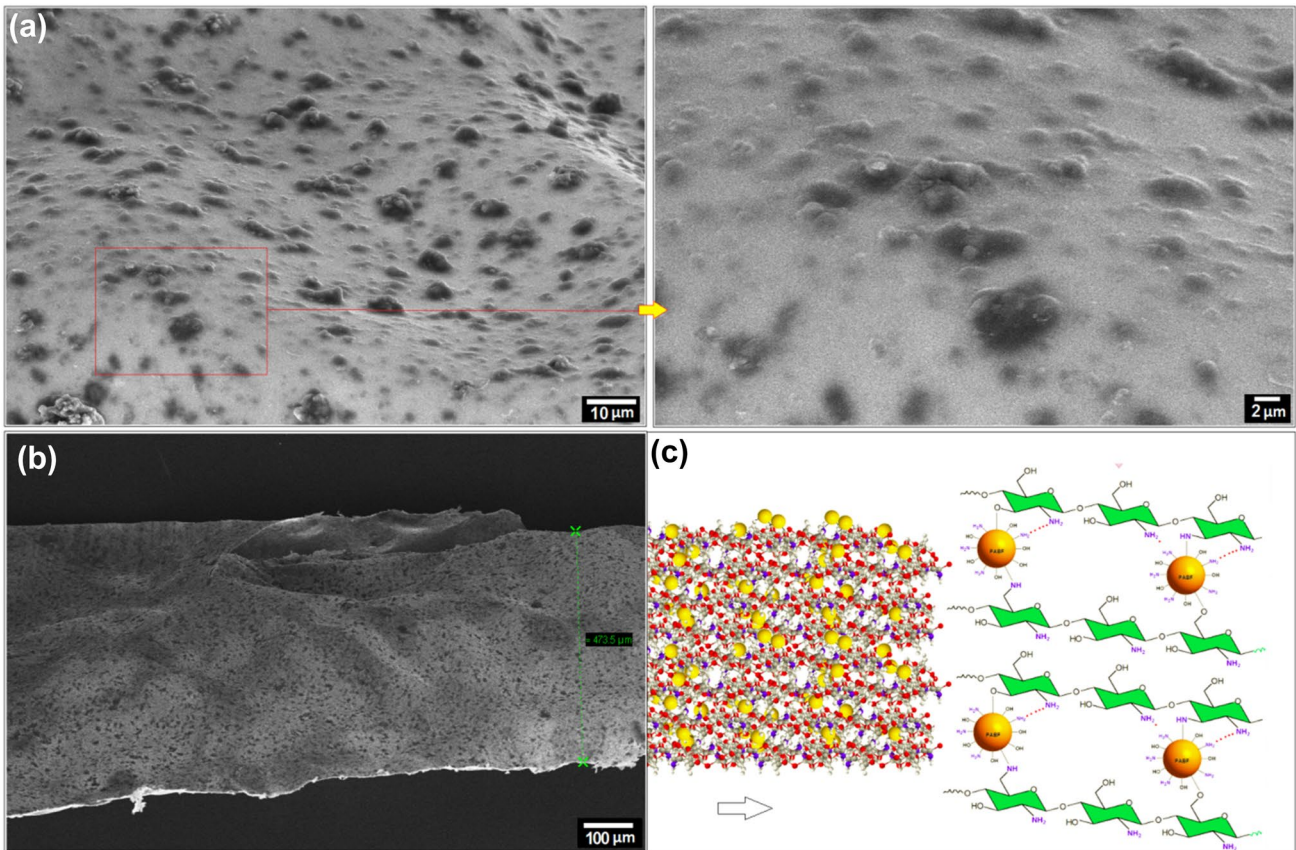


Fig. 5 SEM image of the surface and cross sectional PABF/chitosan nanocomposite

**Table 2** Complete design matrix with observed and predicted experimental response values

Run	Independent variables						Removal efficiency (%)	
	pH, $X_1$		Nanoparticle dose, $X_2$		Initial concentration, $X_3$		Observed	Predicted
	Coded	Actual	Coded	Actual (g)	Coded	Actual (mg/L)		
1	1	6	0	0.046	- 1	50	98.856	99.787
2	1	6	1	0.090	0	100	92.799	93.128
3	0	4.5	1	0.090	- 1	50	91.950	89.890
4	- 1	3	- 1	0.002	0	100	65.029	64.931
5	0	4.5	0	0.046	0	100	89.283	86.820
6	0	4.5	- 1	0.002	- 1	50	82.790	84.735
7	1	6	0	0.046	1	150	88.877	89.925
8	0	4.5	1	0.090	1	150	72.653	72.306
9	- 1	3	0	0.046	1	150	59.861	59.161
10	- 1	3	0	0.046	- 1	50	85.284	84.467
11	1	6	- 1	0.002	0	100	95.771	93.925
12	0	4.5	- 1	0.002	1	150	67.152	67.151
13	0	4.5	0	0.046	0	100	85.272	86.820
14	0	4.5	0	0.046	0	100	86.367	86.820
15	- 1	3	1	0.090	0	100	73.960	76.038

**Table 3** Sequential model fitting for the lead adsorption on PABF/chitosan nanocomposite

Source	Sequential model sum of squares					Comment
	Sum of squares	Degree of freedom	Mean square	F value	p value > F	
Mean vs. Total	101,800	1	101,800	-	-	-
Linear vs. Mean	1733.44	3	577.81	25.86	< 0.0001	-
2FI vs. Linear	98.40	3	32.80	1.78	0.2285	-
Quadratic vs. 2FI	123.16	3	41.05	8.48	0.0209	Suggested
Cubic vs. Quadratic	15.61	3	5.20	1.21	0.4822	Aliased
Residual	8.60	2	4.30	-	-	-
Total	103,800	15	6920.64	-	-	-

Source	Lack of fit tests					Remark
	Sum of squares	Degree of freedom	Mean square	F value	p value > F	
Linear	237.17	9	26.35	6.13	0.1481	-
2FI	138.76	6	23.13	5.38	0.1650	-
Quadratic	15.61	3	5.20	1.21	0.4822	Suggested
Cubic	0.000	0	-	-	-	Aliased
Pure Error	8.60	2	4.30	-	-	-

Source	Model Summary Statistics					Remark
	Std. Dev	R <sup>2</sup>	R <sup>2</sup> <sub>adj</sub>	Predicted R <sup>2</sup>	PRESS	
Linear	4.73	0.8758	0.8420	0.7700	455.24	-
2FI	4.29	0.9255	0.8697	0.7545	485.90	-
Quadratic	2.20	0.9878	0.9658	0.8641	269.04	Suggested
Cubic	2.07	0.9957	0.9696	-	-	Aliased



**Table 4** ANOVA for response surface full quadratic model

Source	Sum of squares	Degree of freedom	Mean square	F value	p value > F
Model	1955.00	9	217.22	44.88	0.0003
X <sub>1</sub> -pH	1061.87	1	1061.87	219.37	<0.0001
X <sub>2</sub> -C <sub>n</sub>	53.15	1	53.15	10.98	0.0212
X <sub>3</sub> -C <sub>0</sub>	618.42	1	618.42	127.76	<0.0001
X <sub>1</sub> X <sub>2</sub>	35.42	1	35.42	7.32	0.0425
X <sub>1</sub> X <sub>3</sub>	59.63	1	59.63	12.32	0.0171
X <sub>2</sub> X <sub>3</sub>	3.35	1	3.35	0.69	0.4435
X <sub>1</sub> <sup>2</sup>	0.23	1	0.23	0.048	0.8354
X <sub>2</sub> <sup>2</sup>	86.27	1	86.27	17.82	0.0083
X <sub>3</sub> <sup>2</sup>	45.34	1	45.34	9.37	0.0281
Residual	24.20	5	4.84	–	–
Lack of Fit	15.61	3	5.20	1.21	0.4822
Pure Error	8.60	2	4.30	–	–
Cor Total	1979.20	14	–	–	–

$R^2=0.9878, R^2_{adj}=0.9658, R^2_{pre}=0.8641$

**Table 5** ANOVA for response surface reduced quadratic model

Source	Sum of squares	Degree of freedom	Mean square	F value	p value > F
Model	1951.42	7	278.77	70.24	<0.0001
X <sub>1</sub> -pH	1061.87	1	1061.87	267.55	<0.0001
X <sub>2</sub> -C <sub>n</sub>	53.15	1	53.15	13.39	0.0081
X <sub>3</sub> -C <sub>0</sub>	618.42	1	618.42	155.82	<0.0001
X <sub>1</sub> X <sub>2</sub>	35.42	1	35.42	8.92	0.0203
X <sub>1</sub> X <sub>3</sub>	59.63	1	59.63	15.03	0.0061
X <sub>2</sub> <sup>2</sup>	86.09	1	86.09	21.69	0.0023
X <sub>3</sub> <sup>2</sup>	45.11	1	45.11	11.37	0.0119
Residual	27.78	7	3.97	–	–
Lack of Fit	19.19	5	3.84	0.89	0.6037
Pure Error	8.60	2	4.30	–	–
Cor Total	1979.20	14	–	–	–

$R^2=0.9860, R^2_{adj}=0.9719, R^2_{pre}=0.9208$

**BBD Method**

The BBD is a suitable approach to expand a polynomial regression model for analyzing the interaction of variables and finding the most effective variables on the adsorption process. A three-factor, three-level Box–Behnken statistical design requires 15 experiments. Table 2 presents the complete design matrix along with measured and predicted response values. The experimental error is determined using three replicates at the center point. The highest lead removal efficiency was found to be 98.86%.

■ pH ■ adsorbent dose ■ Initial lead concentration ■ Interactions

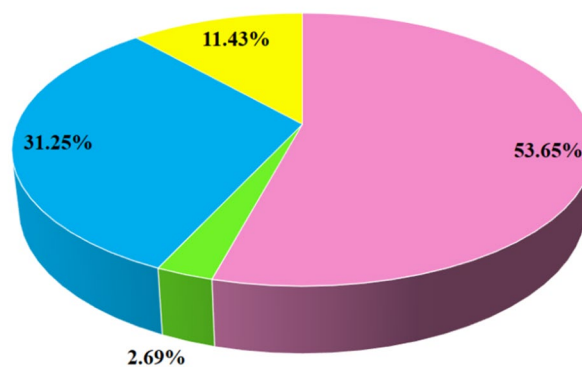


**Fig. 6** Percent contribution of various parameters on lead removal efficiency by PABF/chitosan nanocomposite

### Regression Model and Statistical Analysis

To predict the optimum point, an empirical quadratic polynomial model was derived using Eq. (3):

$$Y = b_0 + \sum_{i=1}^k b_i X_i + \sum_{i=1}^k b_{ii} X_i^2 + \sum_{i=1}^{k-1} \sum_{j=i+1}^k b_{ij} X_i X_j \quad (3)$$

which Y as a response variable is removal efficiency (%);  $b_0$  is a constant coefficient;  $b_i$  stands for the linear regression coefficients;  $b_{ii}$  and  $b_{ij}$  represent the square and interaction coefficients, respectively.  $X_i$  and  $X_j$  are the coded notations of experimental variables and k is the total number of the independent variables (Abedi and Ebrahimzadeh 2013). The BBD from RSM series was selected to assessed the influences of process variables such as nanoparticle dose, initial pH, and initial Pb(II) concentration on the Pb(II) removal efficiency. Interactive, Linear, quadratic, and cubic models were chosen to scrutinize the interaction effects of the mentioned factors. Three different tests including lack of fit (LOF) tests, sequential model sum of squares, and model summary statistics were considered to determine the adequacy of the models representing Pb(II) removal by PABF/chitosan nanocomposite. Table 3 presents the adequacy results.

Regarding Table 4, one can see that quadratic model is the most appropriate model for the Pb(II) removal by nanocomposite. The tests for adequacy of the model was evaluated via analysis of variance (ANOVA).

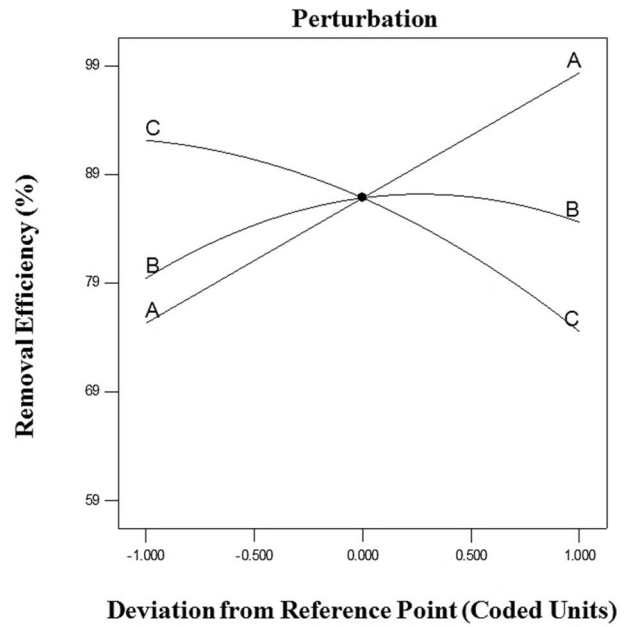


Fig. 8 Perturbation plots; A initial solution pH, B nanoparticle dose and C initial lead concentration

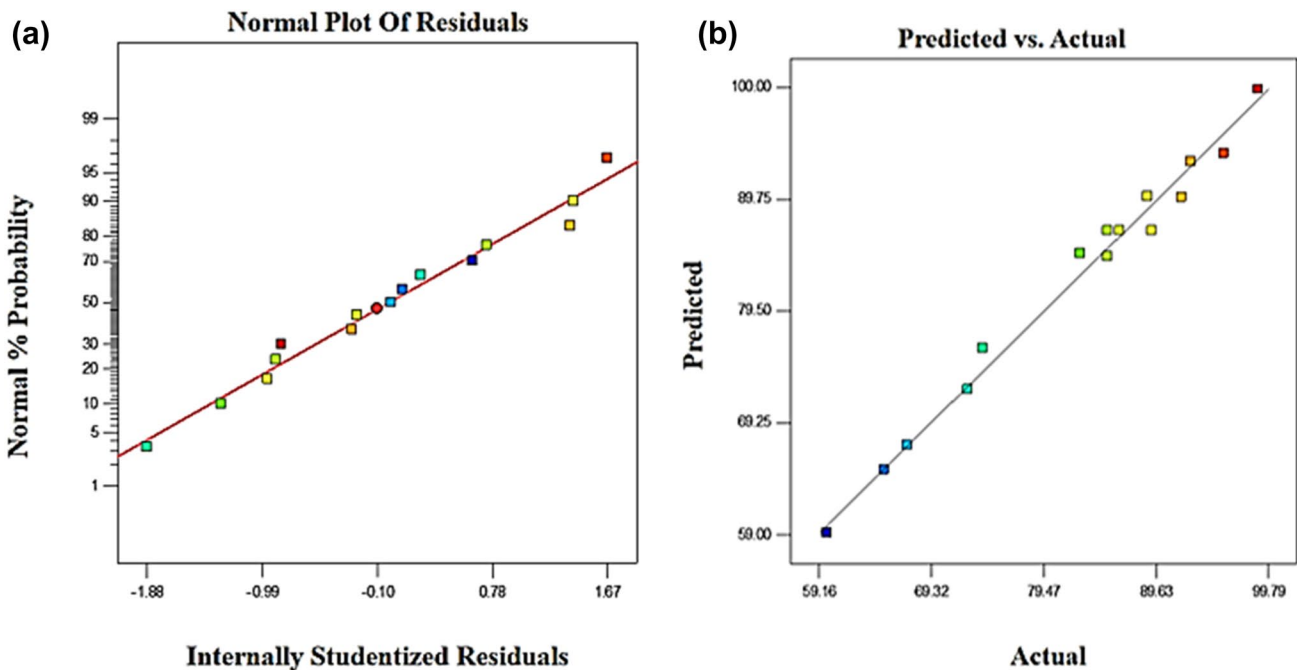


Fig. 7 a Normal % probability against residual error, b Predicted response against actual response

### Analysis of Variance Study

ANOVA was performed to check the compatibility and significance of the model (Da'na and Sayari 2011). The ANOVA for the Pb adsorption quadratic model of nano-composite is depicted in Table 4. The significance of the terms in the regression models is not identical. The  $F$  and  $p$  values were calculated to determine the significance of each coefficient. The lower the  $p$ -value and the bigger the  $F$

value, the more profound significance of the corresponding coefficients. As presented in Table 4, the  $F$  value of 44.88 implied the model significant. Significant terms of the model were found to be  $X_1$ ,  $X_2$ ,  $X_3$  and interactions  $X_1X_2$ ,  $X_1X_3$ ,  $X_2^2$  and  $X_3^2$ . Non-significant terms were found from the  $p$  values  $\geq 0.050$ . Thus model reduction was applied to tailor the model; for such a purpose  $X_1^2$  and  $X_2X_3$  were eliminated. As a result, the model  $F$  value was 70.24 (Table 5). The LOF is a special test to investigate the adequacy of a model fit, and non-significant LOF is favorable. In the present study the LOF is not significant compared to the pure error,

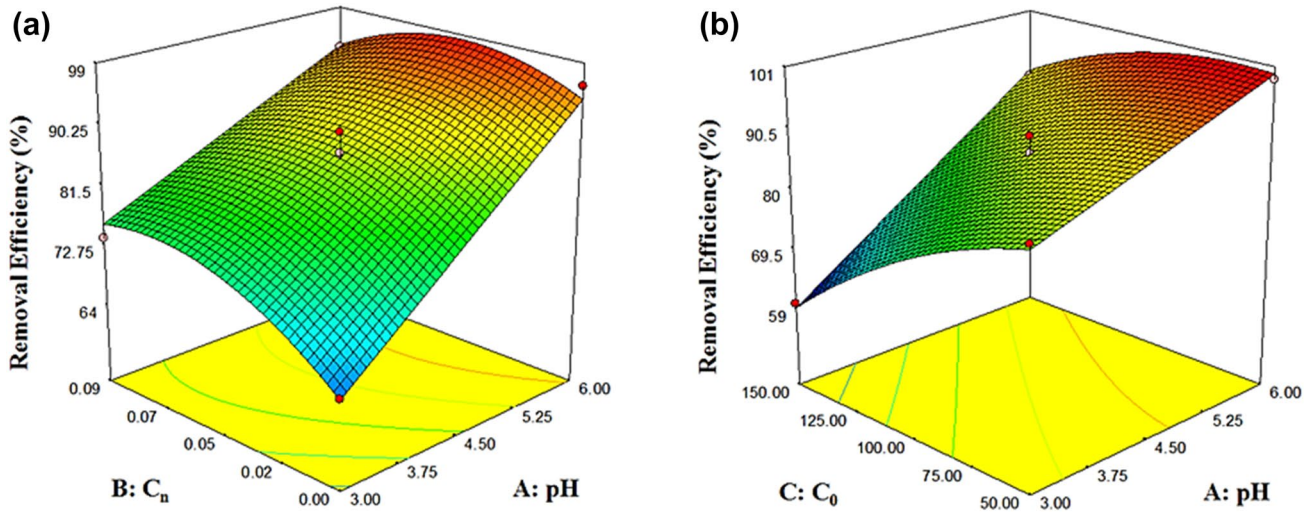


Fig. 9 3-D surface plots for interactive effect of **a** pH and adsorbent dose, **b** pH and initial concentration

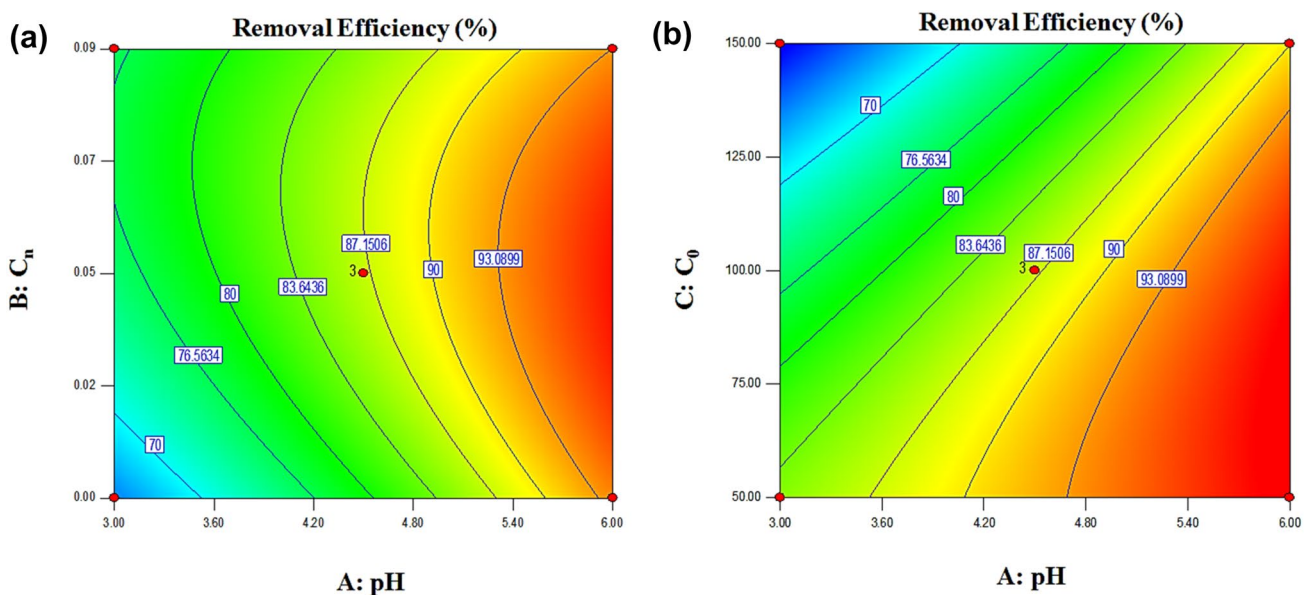


Fig. 10 Contour plots exhibiting the interactive effects between two independent variables (other variables were held at their respective center levels); **a** initial pH of solution (pH,  $X_1$ ) and nanosorbent dose

( $C_n$ ,  $X_2$ ), **b** initial pH of solution (pH,  $X_1$ ) and initial concentration of Pb(II) ions ( $C_n$ ,  $X_3$ )

demonstrating a desirable response to the model. The correlation coefficients  $R^2$  and  $R^2_{adj}$  were calculated to inspect the adequacy of the model. In statistical modelling, by eliminating the non-significant terms, the coefficient of determination is declined; therefore a high R-squared value does not inevitably mean a good regression model. Hence, the  $R^2_{adj}$  value is used to examine the goodness of fitting of a regression model (Habibi and Vahabzadeh 2013; Zhang and Zheng 2009). Statistical analysis was performed to investigate if the regression models conform to experimental data. In this work, a high R-squared value (0.986) elucidated a high correlation and dependency between the experimental and the predicted values of response. The value of  $R^2_{adj}$  (0.972) showed that the independent variables had a 97% contribution to the total variation for Pb(II) removal efficiency and only ~3% cannot be justified by the model. Equation (4) represents the Pb(II) removal response function:

$$Y = 86.82 + 11.52X_1 + 2.58X_2 - 8.79X_3 - 2.98X_1X_2 + 3.86X_1X_3 - 4.81X_2^2 - 3.48X_3^2 \quad (4)$$

Considering the coefficients in Eq. (4), it can be concluded that removal efficiency is enhanced with the pH ( $X_1$ ) and  $C_n$  ( $X_2$ ) and is declined with  $C_0$  ( $X_3$ ). It is obvious that the initial pH ( $X_1$ ) has a greater impact on Pb(II) adsorption than nanoparticle dose ( $X_2$ ) and initial concentration ( $X_3$ ), which is in coincidence with contribution percentages depicted in Fig. 6.

The normality of the residuals is also analyzed as shown in Fig. 7a. Proximity of data points to a straight line means a normal distribution of model errors.

Figure 7b illustrates the actual and predicted values of percentage removal of Pb ions. The points of all actual and predicted responses fell in a 45° line, demonstrating a good agreement between the experimental and the predicted values.

The perturbation plot was utilized to investigate the influence of three factors concurrently on the lead adsorption (Fig. 8). In the perturbation plot, removal efficiency was plotted by altering only one factor over its range while holding all other factors constant at the coded zero level. As depicted in Fig. 8, initial pH (A), nonabsorbent dose (B) and initial concentration (C) are the influential factors for attaining maximum lead removal efficiency. A steep slope in solution pH curve displays that Pb(II) removal percentage is very pH-sensitive, whereas a nanosorbent dosage-insensitive behavior was disclosed in the relatively flat curves for nanosorbent dosage. In addition, the related perturbation plot reveals that the initial concentration (C) can significantly affect the adsorption process; albeit this is not as effective as pH.

### Comparative Effects of Process Variables on Pb(II) Removal Efficiency

The 2D contours and 3D response surface plots that illustrate the relationship between independent and dependent variables are very beneficial to perusal the interaction effects

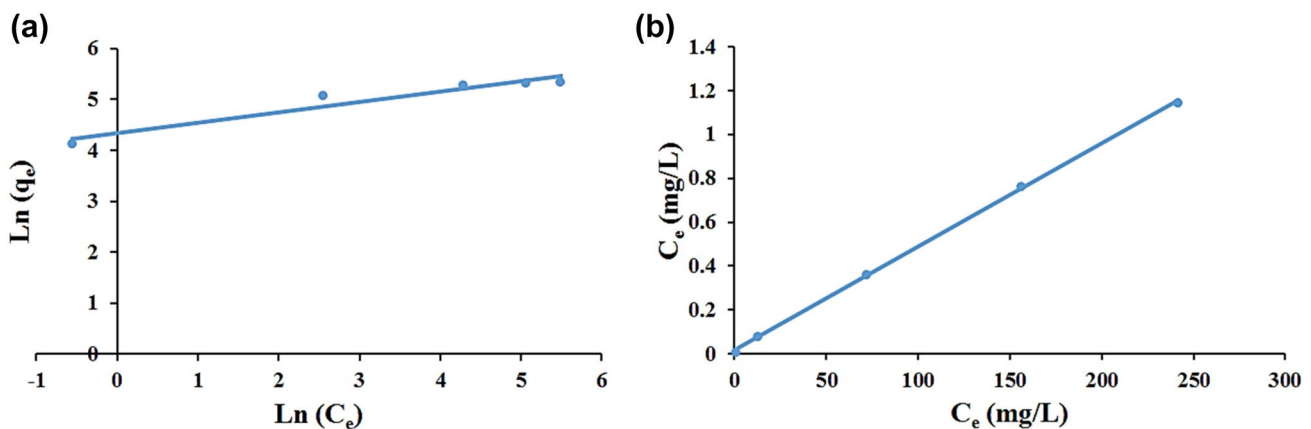
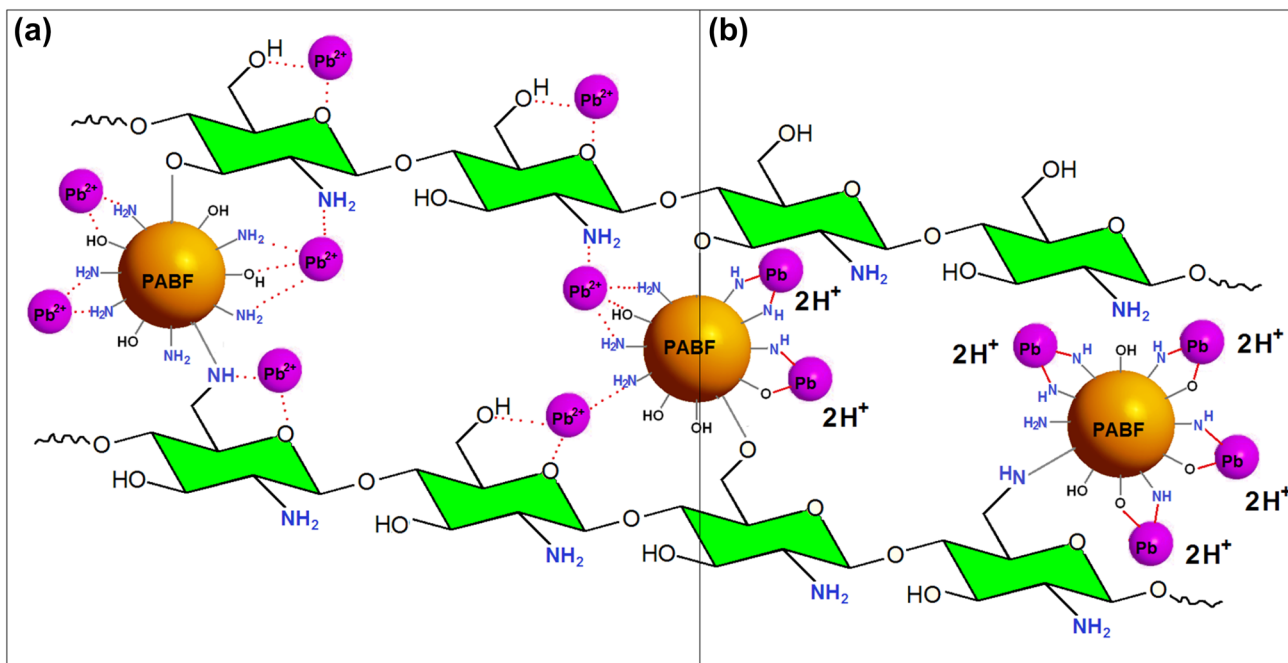


Fig. 11 Freundlich (a) and Langmuir (b) isotherms for Pb(II) adsorption onto PABF/chitosan nanocomposite

**Table 6** Langmuir and Freundlich isotherm model parameters for adsorption of Pb(II) on PABF/chitosan nanocomposite

Langmuir				Freundlich		
$Q_{max}$ (mg/g)	$b$ (L/mg)	$R^2$	$R_L$	$K_f$ (mg/g)	$n$ (L/mg)	$R^2$
212.76	0.2671	0.9996	0.009–0.0696	77.25	4.92	0.9307



**Fig. 12** Mechanism of Pb(II) adsorption onto the PABF/chitosan nanocomposite, **a** complex formation mechanism and **b** ion exchange mechanism

of the factors on the responses. These kinds of plots display the influences of two factors on the response at a specified time. Thus, in the current study, the model given in Eq. (4) was used to visualize the measured responses in the form of 3D surface plots. The relationship between the independent and the dependent variables was further elucidated by plotting contours. Figures 9 and 10 depict the 3D response surfaces and the related contour plots as the functions of two variables at the center points of other variables, respectively.

### Sorption Isotherms

For explaining the interaction between sorbent and sorbate, equilibrium isotherm is often assumed which gives the capacity of a sorbent for a sorbate (Ho 2006). Freundlich and Langmuir isotherm models are the most commonly isotherms. The Freundlich isotherm, assumes the adsorption characteristics of the heterogeneous surface with unrestricted adsorption sites of different adsorption energies. Langmuir model, on the other hands, describes that adsorption takes place on a homogeneous surface with sorption sites of similar surface energies (Naeem et al. 2007; Wang et al. 2017; Shahzad et al. 2017; Lv et al. 2017). Equations (5) and (6) depicts the Freundlich and Langmuir models, respectively:

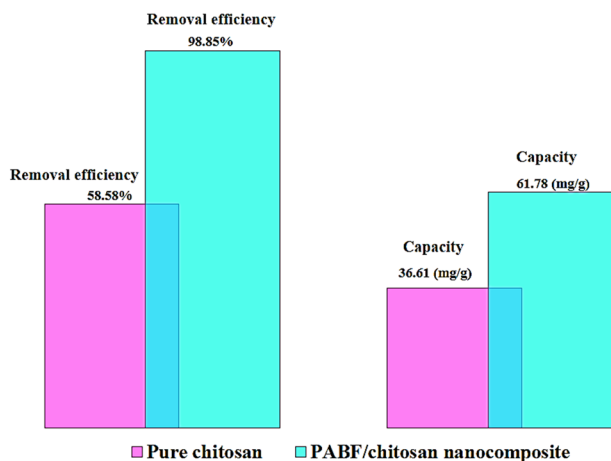


**Fig. 13** Comparison of the removal efficiency and capacity of pure chitosan and PABF chitosan film

$$q_e = K_f C_e^{1/n} \tag{5}$$

$$q_e = \frac{Q_{max} b C_e}{1 + b C_e} \tag{6}$$

where  $C_e$  is the equilibrium concentration of adsorbate in solution (mg/L),  $q_e$  is the equilibrium sorption capacity

**Table 7** Results of recent research on Pb<sup>2+</sup> removal by other adsorbents

Researcher(s)	Adsorbent	Removal efficiency (%)	Experimental conditions
The authors of the present work	Para-amino benzoate ferroxane/Chitosan Nanocomposite	98.27	T=25 °C pH=6 Adsorbent dosage: 0.04 g Conc. = 75 mg/L
Jasim et al. (2022)	Modified chitosan Schiff base@Fe/NiFe	97	T=25 °C pH=4 Adsorbent dosage: 0.05 g Conc. = 75 mg/L
Ghahremani et al. (2021)	Modified silica aerogel	75	T=25 °C pH=4 Adsorbent dosage: 1.4 g/L Conc. = 50 mg/L
Gao et al. (2020)	Oxidized rape straw biochars	97.4	T=25 °C pH=2 Conc. = 1 mol/L
Lakkaboyana et al. (2021)	Indonesian Kaolin supported nZVI (IK-nZVI)	98	T=25 °C pH=4.5–6.5 Conc. = 60 mg/L
Ma et al. (2021)	Thermally modified waste concrete powder	93	T=25 °C pH=1–6 Adsorbent dosage: 50 g/L Conc. = 1000 mg/L
Sarojini et al. (2019)	Polypyrrole–iron oxide–seaweed nanocomposite	97.25	T=40 °C pH=5 Adsorbent dosage: 1 g/L Conc. = 100 mg/L
Najaflou et al. (2021)	Cellulose sulfate/chitosan aerogel	92	T=26 °C pH=5 Adsorbent dosage: 2 g/L Conc. = 300 mg/L

**Table 8** Cost estimation of nanoadsorbent preparation

Cost description	Consumed amount	Cost*
Chitosan powder	0.2 g	0.2 × 0.0015 = 0.0003 USD
Acetic acid	9.7 g	9.7 × 0.0007 = 0.0068 USD
FeCl <sub>2</sub> ·4H <sub>2</sub> O	20.0 g	20 × 0.00031 = 0.0062 USD
NaNO <sub>3</sub>	7.0 g	7 × 0.0005 = 0.0035 USD
Hexamethylenetetramine	28.0 g	28 × 0.0017 = 0.0476 USD
4-Aminobenzoic acid	6.0 g	6 × 0.005 = 0.03 USD
Mass of adsorbent synthesized	5.0 g	
Total cost of materials	0.019 USD/g adsorbent	
Total cost of materials	0.019 USD/g adsorbent	

\*Calculated based on the price at 10 Sep, 2022

(mg/g sorbent),  $K_f$  and  $n$  are the Freundlich constants related to adsorption capacity and energy of adsorption, respectively.  $Q_{max}$  and  $b$  are the Langmuir constants representing the adsorption capacity (mg/g) and energy of adsorption (L/mg), respectively. The necessary characteristics of the Langmuir isotherm ( $R_L$ ) are defined as

$$R_L = \frac{1}{1 + bc_0} \quad (7)$$

This result indicated that the empirical Langmuir isotherm surpasses the Freundlich isotherm in explaining the behavior of leads(II) adsorption onto adsorbent, indicating

a monolayer adsorption onto a surface containing a limited quantity of identical sites (Fig. 11; Table 6).

### Adsorption Mechanism onto PABF/Chitosan Nanocomposite

Removing cations from the aqueous medium is an intricate process; there are various types of mechanisms such as ion exchange, complexation or chelation, adsorption (physisorption or chemisorption), micro-precipitation, etc. For this purpose, it is beneficial to realize a deep understanding of the functional groups present on the surface of nanocomposite, surface texture and the elemental analysis of materials.

Figure 12 schematizes the Pb(II) adsorption mechanism onto the PABF/chitosan nanocomposite. Adsorption may occur through both complex formation (Fig. 12a) and ion exchange (Fig. 12b) mechanisms. Complex formation occurs since  $Pb^{2+}$  has been chelated by active functional groups (OH,  $NH_2$ ) but ion exchange occurs partly, since amine ( $NH_2$ ) or OH groups on the surface of nanoparticles can easily lose  $H^+$  ions and adsorb lead. However, this is more probable that both of these mechanisms have concerted effect on the adsorption process.

### Optimizing Variables for Pb(II) Removal

To find the optimum values of the opted experiment variables, it is necessary to solve the Eq. (4) and also interpret the response surface contour plots. In this way, the optimal variables were obtained 5.99 ( $X_1 = 0.99$ ) for initial solution pH, 74.48 mg/L ( $X_2 = -0.51$ ) for the initial Pb(II) concentration, and 0.04 g ( $X_3 = -0.04$ ) for nanoparticle dosage with a predicted Pb(II) removal efficiency of around 99.93%. Verifying adsorption experiment was later performed to examine the predicted result. A good coincidence was revealed between the experimental value (98.27%) and the predicted one.

### Adsorption of Pb(II) onto Pure Chitosan Film

Adsorption of Pb(II) onto pure chitosan film was conducted under conditions of  $C_0 = 50$  mg/L, pH = 6, contact time = 24 h, an stirring speed of 200 rpm at room temperature. The adsorption capacity and the removal efficiency were 36.61 mg/g and 58.58%, respectively; whereas the adsorption capacity and the removal efficiency of PABF/chitosan nanocomposite in the same conditions ( $C_n = 0.046$ ) were 98.85% and 61.78 mg/g, respectively. A comparative look at these data confirms Pb(II) uptake improvement by ferroxane nanoparticles-incorporated chitosan film (Fig. 13).

### Comparative Study

Many adsorbents have been used to remove lead from aqueous solutions, each of which has its own advantages and drawbacks. In order to make a reasonable comparison, it is necessary to consider adsorbents whose experimental conditions are similar or close to the experimental conditions of the adsorbent used in this study. Table 7 provides such a comparison between the current adsorbent and some recent adsorbents in the field of lead removal from aqueous solutions. From the data in Table 7, it can be concluded that the adsorbent synthesized in this study showed better lead removal efficiency. This better efficiency has been achieved in conditions of pH, dosage, and in some cases, the temperature of the aqueous solution, which makes it possible to use it on a large scale. In addition, the adsorbent used in this study was synthesized from more available and cheaper raw materials.

### Cost Estimation

Table 8 shows the cost estimation of the synthesis of 1 g of composite adsorbent used in this study, which is based on the price of raw materials. There is little information in the literature on estimating the cost of producing an adsorbent for water/wastewater treatment. The total cost of producing an adsorbent depends on various parameters such as operating conditions, availability of raw materials, and process requirements. It is meaningful to include the mentioned parameters in the pilot and larger scales, and since the adsorbent synthesis in this study was performed on a laboratory scale, the cost of adsorbent production was estimated only based on the price of starting materials. From Table 8, it can be concluded that the production cost of 1 kg of adsorbent is about 19 USD, which is lower compared to commercial activated carbon (more than 20 USD). Meanwhile, it shows a better performance in removing lead compared to many commercial adsorbents.

### Conclusions

The present study has demonstrated the use of Box–Behnken design approach from RSM to achieve the maximum aqueous Pb(II) uptake by PABF/chitosan nanocomposites. The functional groups on the nanoparticles via being crosslinked with chitosan polymer chains improved the adsorption properties. The effect of different parameters including adsorbent amount, initial solution

pH, and initial  $\text{Pb}^{2+}$  concentration was studied. There was a very good agreement between the regression equation and the experimental data. An initial solution pH, an initial Pb concentration of 74.5 mg/L, and an adsorbent mass of 0.04 g were obtained as the optimum conditions. A removal efficiency of 98.27% was measured at optimum conditions, exhibiting a good coincidence with the predicted value (99.93%). The Langmuir isotherm exhibited a better fit compared to Freundlich model, confirming the occurrence of monolayer adsorption.

In the present research, the use of chitosan as an environmentally friendly natural polymer, facile nano-adsorbent synthesis process, easy separation of the adsorbent from water after the adsorption process, and a high adsorption efficiency at pH = 6 (very close to the pH of drinking water) are the most important engineering aspects.

**Supplementary Information** The online version contains supplementary material available at <https://doi.org/10.1007/s41742-022-00481-y>.

**Authors' Contributions** RMM: conceptualization, formal analysis, investigation, methodology, visualization, writing—original draft, and writing—review and editing. SR: conceptualization, formal analysis, investigation, methodology, and writing—original draft. LR: project administration, resources, and supervision. AAD: formal analysis, methodology, visualization, and writing—original draft.

## Declarations

**Conflict of Interest** On behalf of all authors, the corresponding author states that there is no conflict of interest. The authors declare that they have no known competing financial interests or personal relationships that could have appeared to influence the work reported in this paper.

## References

- Abedi H, Ebrahimzadeh H (2013) Imprinted polymer-based extraction for speciation analysis of inorganic tin in food and water samples. *React Funct Polym* 73:634–640. <https://doi.org/10.1016/j.reactfunctpolym.2013.01.011>
- Abou-Shady A, Peng C, Bi J, Xu H, Almeria OJ (2012) Recovery of Pb (II) and removal of  $\text{NO}_3^-$  from aqueous solutions using integrated electro dialysis, electrolysis, and adsorption process. *Desalination* 286:304–315. <https://doi.org/10.1016/j.desal.2011.11.041>
- Ahmed Z, Wu P, Jiang L, Liu J, Ye Q, Yang Q, Zhu N (2020) Enhanced simultaneous adsorption of Cd (II) and Pb (II) on octylamine functionalized vermiculite. *Colloid Surf A-Physicochem Eng Asp* 604:125285. <https://doi.org/10.1016/j.colsurfa.2020.125285>
- Amini M, Younesi H, Bahramifar N, Lorestani AAZ, Ghorbani F, Daneshi A, Sharifzadeh M (2008) Application of response surface methodology for optimization of lead biosorption in an aqueous solution by *Aspergillus niger*. *J Hazard Mater* 154:694–702. <https://doi.org/10.1016/j.jhazmat.2007.10.114>
- Ay F, Catalkaya EC, Kargi F (2009) A statistical experiment design approach for advanced oxidation of Direct Red azo-dye by photo-Fenton treatment. *J Hazard Mater* 162:230–236. <https://doi.org/10.1016/j.jhazmat.2008.05.027>
- Bandaru VVR, Somalanka SR, Mendu DR, Madicherla NR, Chityala A (2006) Optimization of fermentation conditions for the production of ethanol from sago starch by co-immobilized amyloglucosidase and cells of *Zymomonas mobilis* using response surface methodology. *Enzyme Microb Technol* 38:209–214. <https://doi.org/10.1016/j.enzmictec.2005.06.002>
- Boddu VM, Abburi K, Randolph AJ, Smith ED (2008) Removal of copper (II) and nickel (II) ions from aqueous solutions by a composite chitosan biosorbent. *Sep Sci Technol* 43:1365–1381. <https://doi.org/10.1080/01496390801940762>
- Chang M-Y, Juang R-S (2004) Adsorption of tannic acid, humic acid, and dyes from water using the composite of chitosan and activated clay. *J Colloid Interface Sci* 278:18–25. <https://doi.org/10.1016/j.jcis.2004.05.029>
- Chen Y, Cai W, Dang C, Fan J, Zhou J, Liu Z (2020) A facile sol-gel synthesis of chitosan-boehmite film with excellent acid resistance and adsorption performance for Pb (II). *Chem Eng Res Des* 161:332–339. <https://doi.org/10.1016/j.cherd.2020.07.018>
- Celebi H, Gök O (2017) Evaluation of lead adsorption kinetics and isotherms from aqueous solution using natural walnut shell. *Int J Environ Res* 11(1):83–90. <https://doi.org/10.1007/s41742-017-0009-3>
- Çelebi H, Gök G, Gök O (2020) Adsorption capability of brewed tea waste in waters containing toxic lead (II), cadmium (II), nickel (II), and zinc (II) heavy metal ions. *Scient Report* 10:17570. <https://doi.org/10.1038/s41598-020-74553-4>
- Chiou M-S, Ho P-Y, Li H-Y (2004) Adsorption of anionic dyes in acid solutions using chemically cross-linked chitosan beads. *Dyes Pigment* 60:69–84. [https://doi.org/10.1016/S0143-7208\(03\)00140-2](https://doi.org/10.1016/S0143-7208(03)00140-2)
- Crini G, Badot P-M (2008) Application of chitosan, a natural aminopolysaccharide, for dye removal from aqueous solutions by adsorption processes using batch studies: a review of recent literature. *Prog Polym Sci* 33:399–447. <https://doi.org/10.1016/j.progpolymsci.2007.11.001>
- Da'na E, Sayari A. (2011) Optimization of copper removal efficiency by adsorption on amine-modified SBA-15: experimental design methodology. *Chem Eng J* 167:91–98. <https://doi.org/10.1016/j.cej.2010.12.005>
- Dil EA, Ghaedi M, Ghezalbash GR, Asfaram A, Purkait MK (2017) Highly efficient simultaneous biosorption of  $\text{Hg}^{2+}$ ,  $\text{Pb}^{2+}$  and  $\text{Cu}^{2+}$  by Live yeast *Yarrowia lipolytica* 70562 following response surface methodology optimization: kinetic and isotherm study. *J Ind Eng Chem* 48:162–172. <https://doi.org/10.1016/j.jiec.2016.12.035>
- Dolgen D, Necdet Alpaslan M, Delen N (2007) Agricultural recycling of treatment-plant sludge: a case study for a vegetable-processing factory. *J Environ Manage* 84:274–281. <https://doi.org/10.1016/j.jenvman.2006.06.013>
- Fiorito F, Porcedda GE, Brundu L, Passiu C, Atzei D, Ennas G, Elsener B, Fantauzzi M, Rossi A (2022) Calcium carbonate as sorbent for lead removal from wastewaters. *Chemosphere* 296:133897. <https://doi.org/10.1016/j.chemosphere.2022.133897>
- Ge H, Du J (2020) Selective adsorption of Pb (II) and Hg (II) on melamine-grafted chitosan. *Int J Biol Macromol* 162:1880–1887. <https://doi.org/10.1016/j.ijbiomac.2020.08.070>
- Gao R, Xiang L, Hu H, Fu Q, Zhu J, Liu Y, Huang G (2020) High-efficiency removal capacities and quantitative sorption mechanisms of Pb by oxidized rape straw biochars. *Sci Total Environ* 699:134262. <https://doi.org/10.1016/j.scitotenv.2019.134262>
- Gerente C, Lee V, Cloirec PL, McKay G (2007) Application of chitosan for the removal of metals from wastewaters by adsorption—mechanisms and models review. *Crit Rev Environ Sci Technol* 37:41–127. <https://doi.org/10.1080/10643380600729089>
- Gholami A, Moghadassi A, Hosseini S, Shabani S, Gholami F (2014) Preparation and characterization of polyvinyl chloride based nanocomposite nanofiltration-membrane modified by iron oxide





- nanoparticles for lead removal from water. *J Ind Eng Chem* 20:1517–1522. <https://doi.org/10.1016/j.jiec.2013.07.041>
- Ghahremani P, Vakili MH, Nezamzadeh-Ejhi A (2021) Optimization of Pb (II) removal by a novel modified silica aerogel using Quince seed mucilage with response surface methodology. *J Environ Chem Eng* 9(6):106648. <https://doi.org/10.1016/j.jece.2021.106648>
- Habibi A, Vahabzadeh F (2013) Formaldehyde degradation by *Ralstonia eutropha* in an immobilized cell bioreactor. *J Environ Sci Health Part A* 48:1557–1572. <https://doi.org/10.1080/10934529.2013.797304>
- Hasan M, Ahmad A, Hameed B (2008) Adsorption of reactive dye onto cross-linked chitosan/oil palm ash composite beads. *Chem Eng J* 136:164–172. <https://doi.org/10.1016/j.ccej.2007.03.038>
- Ho Y-S (2006) Isotherms for the sorption of lead onto peat: comparison of linear and non-linear methods. *Pol J Environ Stud* 15:81–86
- Hui B, Ye L (2016) Structure of polyvinyl alcohol-g-acrylic acid-2-acrylamido-2-methyl-1-propanesulfonic acid hydrogel and adsorption mechanism for advanced Pb (II) removal. *J Ind Eng Chem* 35:309–317. <https://doi.org/10.1016/j.jiec.2016.01.010>
- Jasim SA, Hachem K, Abdelbasset WK, Yasin G, Suksatan W (2022) Efficient removal of Pb (II) using modified chitosan Schiff base@ Fe/NiFe. *Int J Biol Macromol* 15(204):644–651. <https://doi.org/10.1016/j.jbiomac.2022.01.151>
- Kalyani S, Priya JA, Rao PS, Krishnaiah A (2005) Removal of copper and nickel from aqueous solutions using chitosan coated on perlite as biosorbent. *Sep Sci Technol* 40:1483–1495. <https://doi.org/10.1081/SS-200055940>
- Kayranli Bİ, Gok O, Yilmaz TU, Gok G, Celebi H, Seckin IY, Mesutoglu OC (2022) Low-cost organic adsorbent usage for removing Ni<sup>2+</sup> and Pb<sup>2+</sup> from aqueous solution and adsorption mechanisms. *Int J Environ Sci Technol* 19(5):3547–3564. <https://doi.org/10.1007/s13762-021-03653-z>
- Kim SH, Chung H, Jeong S, Nam K (2020) Identification of pH-dependent removal mechanisms of lead and arsenic by basic oxygen furnace slag: relative contribution of precipitation and adsorption. *J Clean Prod* 279:123451. <https://doi.org/10.1016/j.jclepro.2020.123451>
- Kołodzińska D, Hałas P, Franas M, Hubicki Z (2017) Zeolite properties improvement by chitosan modification—sorption studies. *J Ind Eng Chem* 52:187–196. <https://doi.org/10.1016/j.jiec.2017.03.043>
- Lee HC, Jeong YG, Min BG, Lyoo WS, Lee SC (2009) Preparation and acid dye adsorption behavior of polyurethane/chitosan composite foams. *Fibers Polym* 10:636–642. <https://doi.org/10.1007/s12221-010-0636-1>
- Liu X, Hu Q, Fang Z, Zhang X, Zhang B (2008) Magnetic chitosan nanocomposites: a useful recyclable tool for heavy metal ion removal. *Langmuir* 25:3–8
- Lakkaboyana SK, Khantong S, Asmel NK, Obaidullah S, Kumar V, Kannan K, Venkateswarlu K, Yuzir A, Yaacob WZW (2021) Indonesian Kaolin supported nZVI (IK-nZVI) used for the efficient removal of Pb (II) from aqueous solutions: Kinetics, thermodynamics and mechanism. *J Environ Chem Eng* 9(6):106483. <https://doi.org/10.1016/j.jece.2021.106483>
- Lv L, Chen N, Feng C, Zhang J, Li M (2017) Heavy metal ions removal from aqueous solution by xanthate-modified cross-linked magnetic chitosan/poly(vinyl alcohol) particles. *RSC Adv* 7:27992–28000. <https://doi.org/10.1039/C7RA02810E>
- Mahmoud ME, Abdelwahab MS (2020) Rapid and efficient removal of lead from water by  $\alpha$ -FeOOH/Cellulose/TiO<sub>2</sub> nanocomposite. *Mater Sci Eng B* 262:114689. <https://doi.org/10.1016/j.mseb.2020.114689>
- Mert EH, Yıldırım H, Üzümcü AT, Kavas H (2013) Synthesis and characterization of magnetic polyHIPEs with humic acid surface modified magnetic iron oxide nanoparticles. *React Funct Polym* 73:175–181. <https://doi.org/10.1016/j.reactfunctpolym.2012.09.005>
- Moattari RM, Rahimi S, Rajabi L, Derakhshan AA, Keyhani M (2014) Statistical investigation of lead removal with various functionalized carboxylate ferroxane nanoparticles. *J Hazard Mater* 283:276–291. <https://doi.org/10.1016/j.jhazmat.2014.08.025>
- Mosleh N, Najmi M, Parandi E, Rashidi Nodeh H, Vasseghian Y, Rezania Sh (2022) Magnetic sporopollenin supported polyamine developed for removal of lead ions from wastewater: kinetic, isotherm and thermodynamic studies. *Chemosphere* 300:134461. <https://doi.org/10.1016/j.chemosphere.2022.134461>
- Muñoz AJ, Espínola F, Ruiz E (2016) Removal of Pb (II) in a packed-bed column by a *Klebsiella* sp. 3S1 biofilm supported on porous ceramic Raschig rings. *J Ind Eng Chem* 40:118–127. <https://doi.org/10.1016/j.jiec.2016.06.012>
- Naeem A, Westerhoff P, Mustafa S (2007) Vanadium removal by metal (hydr) oxide adsorbents. *Water Res* 41:1596–1602. <https://doi.org/10.1016/j.watres.2007.01.002>
- Ngah WSW, Ariff NFM, Hanafiah MAKM (2010) Preparation, characterization, and environmental application of crosslinked chitosan-coated bentonite for tartrazine adsorption from aqueous solutions. *Water Air Soil Pollut* 206:225–236. <https://doi.org/10.1007/s11270-009-0098-5>
- Nkutha CS, Shooto ND, Naidoo EB (2020) Adsorption studies of methylene blue and lead ions from aqueous solution by using mesoporous coral limestones. *S Afr J Chem Eng* 34:151–157. <https://doi.org/10.1016/j.sajce.2020.08.003>
- Najafloo S, Rad MF, Baghdadi M, Bidhendi GRN (2021) Removal of Pb (II) from contaminated waters using cellulose sulfate/chitosan aerogel: Equilibrium, kinetics, and thermodynamic studies. *J Environ Manage* 286:112167. <https://doi.org/10.1016/j.jenvman.2021.112167>
- Ma Z, Xue R, Li JS, Zhao Y, Xue Q, Chen Z, Wang Q, Poon CS (2021) Use of thermally modified waste concrete powder for removal of Pb (II) from wastewater: effects and mechanism. *Environ Pollut* 277:116776. <https://doi.org/10.1016/j.envpol.2021.116776>
- Ogunlaja AS, Coombes MJ, Torto N, Tshentu ZR (2014) The adsorptive extraction of oxidized sulfur-containing compounds from fuels by using molecularly imprinted chitosan materials. *React Funct Polym* 81:61–76. <https://doi.org/10.1016/j.reactfunctpolym.2014.04.006>
- Pal DB, Saini R, Srivastava N, Ahmad I, Alshahrani MY, Gupta VK (2022) Waste biomass based potential bioadsorbent for lead removal from simulated wastewater. *Biores Technol* 349:126843. <https://doi.org/10.1016/j.biortech.2022.126843>
- Rahimi S, Moattari RM, Rajabi L, Derakhshan AA (2015) Optimization of lead removal from aqueous solution using goethite/chitosan nanocomposite by response surface methodology. *Colloid Surf A-Physicochem Eng Asp* 484:216–225. <https://doi.org/10.1016/j.colsurfa.2015.07.063>
- Şener M, Reddy D, Kayan B (2014) Biosorption properties of pretreated sporopollenin biomass for lead (II) and copper (II): Application of response surface methodology. *Ecol Eng* 68:200–208. <https://doi.org/10.1016/j.ecoleng.2014.03.024>
- Sarojini G, Venkateshbabu S, Rajasimman M (2021) Facile synthesis and characterization of polypyrrole-iron oxide–seaweed (PPy-Fe<sub>3</sub>O<sub>4</sub>-SW) nanocomposite and its exploration for adsorptive removal of Pb (II) from heavy metal bearing water. *Chemosphere* 278: 130400. <https://doi.org/10.1016/j.chemosphere.2021.130400>
- Shahzad A, Miran W, Rasool K, Nawaz M, Jang J, Lim S-R, Lee DS (2017) Heavy metals removal by EDTA-functionalized chitosan graphene oxide nanocomposites. *RSC Adv* 7:9764–9771. <https://doi.org/10.1039/C6RA28406J>
- Soylak M, Kars A, Narin I (2008) Coprecipitation of Ni<sup>2+</sup>, Cd<sup>2+</sup> and Pb<sup>2+</sup> for preconcentration in environmental samples prior to flame

- atomic absorption spectrometric determinations. *J Hazard Mater* 159:435–439. <https://doi.org/10.1016/j.jhazmat.2008.02.034>
- Tan Y, Chen M, Hao Y (2012) High efficient removal of Pb (II) by amino-functionalized Fe<sub>3</sub>O<sub>4</sub> magnetic nano-particles. *Chem Eng J* 191:104–111. <https://doi.org/10.1016/j.cej.2012.02.075>
- Tavares AP, Cristóvão RO, Loureiro JM, Boaventura RA, Macedo EA (2009) Application of statistical experimental methodology to optimize reactive dye decolorization by commercial laccase. *J Hazard Mater* 162:1255–1260. <https://doi.org/10.1016/j.jhazmat.2008.06.014>
- Tekin K, Uzun L, Şahin ÇA, Bektaş S, Denizli A (2011) Preparation and characterization of composite cryogels containing imidazole group and use in heavy metal removal. *React Funct Polym* 71:985–993. <https://doi.org/10.1016/j.reactfunctpolym.2011.06.005>
- Tran HV, Tran LD, Nguyen TN (2010) Preparation of chitosan/magnetite composite beads and their application for removal of Pb (II) and Ni (II) from aqueous solution. *Mater Sci Eng C* 30:304–310. <https://doi.org/10.1016/j.msec.2009.11.008>
- Valderruten N, Valverde J, Zuluaga F, Ruiz-Durántez E (2014) Synthesis and characterization of chitosan hydrogels cross-linked with dicarboxylic acids. *React Funct Polym* 84:21–28. <https://doi.org/10.1016/j.reactfunctpolym.2014.08.006>
- Wan Ngah W, Teong L, Hanafiah M (2011) Adsorption of dyes and heavy metal ions by chitosan composites: a review. *Carbohydr Polym* 83:1446–1456. <https://doi.org/10.1016/j.carbpol.2010.11.004>
- Wang L, Wang A (2007) Adsorption characteristics of Congo Red onto the chitosan/montmorillonite nanocomposite. *J Hazard Mater* 147:979–985. <https://doi.org/10.1016/j.jhazmat.2007.01.145>
- Wang C, Boithias L, Ning Z, Han Y, Sauvage S, Sánchez-Pérez J-M, Kuramochi K, Hatano R (2017) Comparison of Langmuir and Freundlich adsorption equations within the SWAT-K model for assessing potassium environmental losses at basin scale. *Agric Water Manag* 180:205–211. <https://doi.org/10.1016/j.agwat.2016.08.001>
- Yang H, Lu M, Chen D, Chen R, Li L, Han W (2020) Efficient and rapid removal of Pb<sup>2+</sup> from water by magnetic Fe<sub>3</sub>O<sub>4</sub>@ MnO<sub>2</sub> core-shell nanoflower attached to carbon microtube: adsorption behavior and process study. *J Colloid Interface Sci* 563:218–228. <https://doi.org/10.1016/j.jcis.2019.12.065>
- Yap M, Mubarak N, Sahu J, Abdullah E (2017) Microwave induced synthesis of magnetic biochar from agricultural biomass for removal of lead and cadmium from wastewater. *J Ind Eng Chem* 45:287–295. <https://doi.org/10.1016/j.jiec.2016.09.036>
- Zhang Z, Zheng H (2009) Optimization for decolorization of azo dye acid green 20 by ultrasound and H<sub>2</sub>O<sub>2</sub> using response surface methodology. *J Hazard Mater* 172:1388–1393. <https://doi.org/10.1016/j.jhazmat.2009.07.146>
- Zheng E, Dang Q, Liu C, Fan B, Yan J, Yu Z, Zhang H (2016) Preparation and evaluation of adipic acid dihydrazide cross-linked carboxymethyl chitosan microspheres for copper ion adsorption. *Colloid Surf A-Physicochem Eng Asp* 502:34–43. <https://doi.org/10.1016/j.colsurfa.2016.05.003>
- Zhu H-Y, Jiang R, Xiao L (2010) Adsorption of an anionic azo dye by chitosan/kaolin/γ-Fe<sub>2</sub>O<sub>3</sub> composites. *Appl Clay Sci* 48:522–526. <https://doi.org/10.1016/j.clay.2010.02.003>

Springer Nature or its licensor holds exclusive rights to this article under a publishing agreement with the author(s) or other rightsholder(s); author self-archiving of the accepted manuscript version of this article is solely governed by the terms of such publishing agreement and applicable law.

## Authors and Affiliations

Rozita M. Moattari<sup>1,2</sup>  · Safoora Rahimi<sup>1</sup> · Laleh Rajabi<sup>1</sup>  · Ali Ashraf Derakhshan<sup>3</sup> 

<sup>1</sup> Polymer Research Center, Department of Chemical Engineering, College of Engineering, Razi University, Kermanshah, Iran

<sup>2</sup> Center of Excellence for Membrane Science and Technology, Department of Chemical, Petroleum and Gas Engineering, Iran University of Science and Technology (IUST), Narmak, Tehran, Iran

<sup>3</sup> Environmental Research Center, Department of Applied Chemistry, Razi University, Kermanshah, Iran